Anisotropic Spin Couplings and the Inelastic Neutron Cross Section of $NaNiO_2$

Laura Filion,[1] Catherine Kallin,[1,2] A. John Berlinsky,[1,2] and Eric Mills[1]

[1]*Department of Physics and Astronomy, McMaster University, Hamilton, Ontario, L8S 4M1, Canada*
[2]*Canadian Institute for Advanced Research, 180 Dundas St. W., Toronto, Ontario, M5G 1Z8, Canada*

The anisotropic spin couplings of the Mott insulator $NaNiO_2$ are calculated and are in excellent agreement with experimental neutron scattering data. The anisotropic exchange couplings are determined using perturbation theory where the crystal field and Coulomb interactions are treated exactly while the spin-orbit and tunneling terms are treated perturbatively. The crystal field Hamiltonian associated with the Ni^{3+} d-orbitals is determined in the point charge approximation. The resulting non-degenerate orbital ground state exhibits the expected t_{2g}-e_g splitting allowing for the observed spin 1/2 associated with the Ni ions. The spin wave dispersion relations, and corresponding inelastic neutron scattering cross section are calculated in the linear spin wave approximation. The isotropic exchange couplings are determined by comparing the model Hamiltonian to experiment. Our analysis also suggests that alkali metal - nickel ion substitutions, rather than geometric frustration within the layers, is a likely explanation for the anomalous magnetic behavior observed in $LiNiO_2$.

PACS numbers: 70.10.-w, 75.10.Dg, 75.40.Gb, 75.30.Ds

I. INTRODUCTION

Although antiferromagnetic interactions tend to stabilize long-range Néel ordered states in two and three dimensions, geometric frustration and quantum effects can destabilize such order, favoring paramagnetic liquid-like states.[1] Since this was pointed out by Anderson[2] and Anderson and Fazekas,[3] considerable efforts have been made to discover systems that would exhibit spin-liquid ground states in which the translational symmetry is that of the lattice but where the spin correlations remain short range down to T=0. Such systems may exhibit unusual fractionalized excitations and, if gapped, a new kind of order, called topological order,[4] which connects the ground state degeneracy to the topology of the magnetic sample.

The ideal candidates for such behavior have spin 1/2 to maximize quantum effects, and the spins are arranged on triangle-based lattices, such as triangular, kagome, or pyrochlore so that Néel order is maximally frustrated. Examples which have attracted considerable interest recently include Cs_2CuCl_4,[5,6] κ-$(ET)_2Cu_2(CN)_3$,[7,8] and $LiNiO_2$.[9,10,11] $LiNiO_2$, which is relevant to the present work, consists of spin 1/2 Ni^{3+} ions arranged on stacked triangular layers. If the dominant magnetic couplings in $LiNiO_2$ were, in fact, antiferromagnetic, then this would be an ideal system for studying the competition between Néel order and spin-liquid behavior. The fact that magnetic ordering has not been observed in this system down to very low temperatures reinforces the idea that ordering is suppressed by frustration and quantum effects. In the present work we study the nature of the magnetic interactions in a closely related compound, $NaNiO_2$ which has an orbitally and magnetically ordered ground state and for which inelastic neutron scattering data exists. Our results, which elucidate the magnetic behavior in $NaNiO_2$, also shed some light on what might be happening in $LiNiO_2$.

$LiNiO_2$ and $NaNiO_2$ are Mott insulators which are isostructural at high temperatures but have significantly different low temperature behavior. Above about 480K, each has a two-fold orbital degree of freedom and a two-fold spin degree of freedom (Kramer's degeneracy). At low temperatures both materials should undergo a cooperative Jahn-Teller structural transition to remove the orbital degree of freedom, as well as a magnetic ordering transition to remove the Kramers degeneracy. $NaNiO_2$ behaves as predicted,[12,13] however, no measurements to date have found signs of either a cooperative Jahn-Teller Effect or magnetic ordering in $LiNiO_2$,[13] although a *local* Jahn-Teller transition may have been observed in $LiNiO_2$ by x-ray absorption fine structure measurements[14] and neutron scattering measurements.[15]

The nature of the magnetic interactions in $LiNiO_2$ and $NaNiO_2$ materials have been debated for some time. Both materials are composed of alternating triangular planes of NiO and MO, where M is either Li or Na respectively (see Fig. 1). As $LiNiO_2$ does not order magnetically, it has been proposed that the couplings in the triangular Ni planes are antiferromagnetic.[16] This, however, contradicts the Goodenough rules which predict a ferromagnetic coupling for the nearly 90° Ni-O-Ni bonds in the Ni planes.[17] Additionally, the Curie-Weiss temperatures of $LiNiO_2$ and $NaNiO_2$ are $\Theta \approx 26$ K and $\Theta \approx 36$ K respectively,[18] indicating that the interactions are predominately ferromagnetic. As the in-plane Ni-O-Ni superexchange is expected to be much larger than the interplane Ni-O-O-Ni exchange interaction, an antiferromagnetic in-plane exchange interaction would not be expected. In keeping with the predictions from the Goodenough rules, magnetization and magnetic susceptibility measurements were used to determine the isotropic spin interactions.[12] The in-plane ferromagnetic interaction was found to be approximately ten times the interplane antiferromagnetic coupling.[12] Additionally, inelastic neutron scattering data on a powder sample of $NaNiO_2$ has been shown to be consistent with in-plane

a	5.3208 Å	β	110.49°
b	2.8440 Å	x_0	0.282 Å
c	5.5818 Å	y_0	0.799 Å

TABLE I: Crystal parameters for $NaNiO_2$ in the low temperature phase (corresponding to the crystallographic space group $C2/m$).[18]

ferromagnetic interactions and interplane antiferromagnetic interactions - provided an easy plane anisotropy is introduced to the Hamiltonian,[19] although the source of the anisotropy was not determined. Recently, however, there has been controversy regarding the in-plane exchange interactions. Vernay *et al.* propose that there are both antiferromagnetic and ferromagnetic exchange interactions in the NiO planes.[9] It is therefore important to determine if the current experimental data contains sufficient information to distinguish between the two proposals, starting with the question of whether the anisotropy required to explain the inelastic neutron scattering data is theoretically justified.

The goal of this paper is to determine the anisotropy associated with the in-plane Ni-O-Ni superexchange and compare the result to the inelastic neutron scattering data. A number of authors have used perturbation theory to determine the anisotropic spin couplings[20,21,22,23] associated with the spin orbit interaction; in this paper, perturbation theory is used to determine the magnitude of the anisotropy associated with the spin-orbit interaction and to calculate the corresponding inelastic neutron cross section. Using a point charge method, we calculate the crystal field splittings of the orbital ground state and, based on this orbital ordering, invoke perturbation theory to determine an effective spin Hamiltonian for $NaNiO_2$. Comparing the results to experiments, we find only a slight modification of the anisotropic Hamiltonian used by Lewis *et al.*[19] and similar exchange couplings.

The paper is organized as follows: In Sec. II the anisotropic spin couplings are calculated; in Sec. III linear spin wave theory is used to determine the spin wave spectrum; in Sec. IV the inelastic neutron cross section is determined and compared to experimental results; and in Sec. V there is a summary and discussion of the results.

II. ANISOTROPIC SPIN COUPLINGS

In its magnetically ordered phase (i.e. below ∼20 K), $NaNiO_2$ is monoclinic and described by the crystallographic space group $C2/m$. The crystal parameters have been determined[18] and are given in Table I. The Ni ions are located at positions $2a$ which have site symmetry $2/m$ and occur at positions (0,0,0) and $(1/2, 1/2, 0)$. The O ions are located at position $4i$ with site symmetry m and occur at $(x_0, 0, z_0)$, $(1/2 + x_0, 1/2, z_0)$, $(\bar{x_0},\ 0,\ \bar{z_0})$ and $(1/2+\bar{x_0},\ 1/2,\ \bar{z_0})$ (see Fig. 1). Each Ni-Ni nearest-neighbor and next-nearest-neighbor bond is centered at

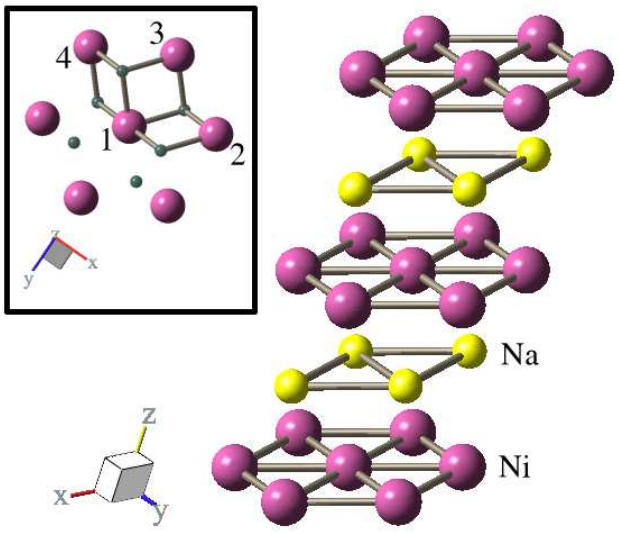

FIG. 1: The main figure shows the structure of $NaNiO_2$ in its low temperature phase (excluding O ions) while the inset depicts the NiO planes. From the inset, note that there are two paths via distinct O ions for Ni-Ni electron hopping and three different possible Ni-Ni bonds: between the Ni ions labeled 1 and 2, 1 and 3, and 1 and 4.

an inversion center of the crystal. Thus the only type of anisotropy expected in this material is symmetric exchange anisotropy,[24] and the Hamiltonian will have the form:

$$H = \sum_{i,j} J_{ij}\mathbf{S}_i \cdot \mathbf{S}_j + \mathbf{S}_i \mathbf{A}_{ij} \mathbf{S}_j, \qquad (1)$$

where J_{ij} is the isotropic spin coupling and $\mathbf{A}_{ij}$ is a symmetric matrix proportional to the square of the spin-orbit interaction containing the anisotropic spin couplings.

A. Crystal Field

As in many superexchange calculations we make the assumption that the Ni ions are well described by localized orbitals. Due to the near cubic symmetry of $NaNiO_2$, a natural choice of basis states for the Ni d-orbitals are the cubic states:

$$|3z^2 - r^2\rangle,\ \ |x^2 - y^2\rangle,\ \ |xz\rangle,\ \ |yz\rangle,\ \ |xy\rangle. \qquad (2)$$

The static crystal field is modeled by treating each ion in the system as a point charge (Ni^{3+}, O^{2-}, Na^{1+}), and calculating the corresponding Coulomb energy. The Ewald summation technique is used to determine the full Madelung sum over the crystal. For a complete description of the method, see Appendix A. The eigenstates and eigenenergies which diagonalize the resulting Hamiltonian are shown in Table II. As is evident from Table II, the crystal field Hamiltonian is block diagonal in the

cubic states: two states consist of linear combinations of yz and xy and the remaining three states consist of linear combinations of x^2-y^2, $3z^2-r^2$, and xz. This is to be expected since the Hamiltonian commutes with the symmetry operator (denoted $\mathbf{R}$) associated with the xz mirror plane at $y=0$ which obeys the eigenequations:

$$\mathbf{R}\big|x^2-y^2\big\rangle = \big|x^2-y^2\big\rangle, \quad (3)$$
$$\mathbf{R}\big|3z^2-r^2\big\rangle = \big|3z^2-r^2\big\rangle, \quad (4)$$
$$\mathbf{R}\big|xz\big\rangle = \big|xz\big\rangle, \quad (5)$$
$$\mathbf{R}\big|yz\big\rangle = -\big|yz\big\rangle, \quad (6)$$
$$\mathbf{R}\big|xy\big\rangle = -\big|xy\big\rangle. \quad (7)$$

Hence, both the Hamiltonian and $\mathbf{R}$ can be diagonalized simultaneously.

The orbital ordering seen in Table II shows the t_{2g}-e_g splitting expected from the Jahn Teller distortion. In the ground state, each Ni^{3+} ion contains seven electrons: the t_{2g} orbitals are completely filled and one electron is in the e_g sector. For the purpose of the perturbative calculation, the t_{2g} orbitals are assumed to be inert, and each Ni^{3+} is modeled by two nondegererate orbitals containing a single electron.

B. Perturbation Theory

The perturbative method used is based on the calculations by Schmitz *et al.* who determined the anisotropic spin couplings in $LaTiO_3$[20] and $YTiO_3$.[21] Our goal is to calculate the exchange coupling parameters in Eq. (1) for the in-plane interactions. According to the Good-enough rules, the in-plane interactions should be much larger than the interplane couplings, so it is expected that nearest neighbor Ni ions within the NiO planes will make the largest contribution to the anisotropy. Additionally, the exchange path for the interplane couplings is more complicated as there are four neighboring O ions involved in the hopping. As the results of the calculation for the interplane anisotropy would be much smaller and less accurate we will not pursue it further. In Sec. III the derived anisotropic interactions are used to determine the corresponding isotropic interactions by comparing the results to experiment. We shall not attempt to compare the isotropic coupling constants to experimental results, since, as has been noted in similar calculations, while perturbation theory accurately approximates the anisotropy, it is insufficient to determine the isotropic couplings.[20,21,23,25] A good description of the problem is found in Ref. 23 where the authors compared exact diagonalization results with a perturbative calculation on the cuprates. While they found good agreement on the anisotropic terms, the two methods produced different results for the isotropic coupling.

The effective couplings (J_{ij} and $\mathbf{A}_{ij}$ in Eq. (1)) occur between nearest neighbor Ni ions. Hence all terms in the perturbative expansion will affect Ni ions in pairs (labeled i and j) and, as such, it is only necessary to include two Ni ions in the calculation. A typical term in the perturbative expansion hops an electron from site i to site j and back. Thus, there are two distinct sectors in our calculation, the Ni^{3+} sector where each Ni site has one electron in e_g orbitals, and the Ni^{2+} sector, where one Ni ion of the pair has no electrons and the other has two electrons shared between the e_g orbitals.

E(eV)	$\|3z^2-r^2\rangle$	$\|x^2-y^2\rangle$	$\|xz\rangle$	$\|yz\rangle$	$\|xy\rangle$
-0.1730	0.1530	-0.7558	-0.6367	0	0
-0.1337	0.8816	-0.1867	0.4335	0	0
-0.0838	0	0	0	-0.4288	-0.9034
0.1414	-0.4464	-0.6277	0.6377	0	0
0.2494	0	0	0	-0.9034	0.4288

TABLE II: Crystal Field States

The unperturbed Hamiltonian includes a crystal field term and the Coulomb interaction between elections on a doubly occupied e_g-shell. The crystal field Hamiltonian is given by

$$H_{CF} = \sum_{i\alpha\sigma} E_\alpha c^\dagger_{i\alpha\sigma} c_{i\alpha\sigma}, \quad (8)$$

where $c^\dagger_{i\alpha\sigma}$ ($c_{i\alpha\sigma}$) creates (annihilates) an electron on site i, in orbital α with spin σ. The zero of the crystal field energy is chosen so that it is zero in the ground state, when there is one electron in orbital $\alpha=1$ at each Ni site. Hence, from Table II, we have $E_1 = 0$eV and $E_2 = 0.1$eV.

The Coulomb Hamiltonian, including both direct and exchange interactions, is given by:

$$H_C = \sum_{\substack{i\alpha\alpha'\\ \beta\beta'}} \sum_{\sigma\sigma'} U_{i\alpha\alpha'\beta\beta'} c^\dagger_{i\alpha\sigma} c^\dagger_{i\beta\sigma'} c_{i\beta'\sigma'} c_{i\alpha'\sigma}, \quad (9)$$

where $U_{i\alpha\alpha'\beta\beta'}$ is evaluated from the Racah parameters[26] (see Table III) and written in terms of states which diagonalize the crystal field Hamiltonian.

The unperturbed Hamiltonian in the Ni^{3+} sector is diagonalized by the crystal field states found in Table II. In the Ni^{2+} sector, the crystal field and Coulomb terms are diagonalized in terms of the following spin singlets and triplets:

$$\Psi_1^{T\dagger}(i\sigma\sigma') = \frac{1}{\sqrt{2}}\left(c^\dagger_{i1\sigma}c^\dagger_{i2\sigma'} + c^\dagger_{i1\sigma'}c^\dagger_{i2\sigma}\right), \quad (10)$$
$$\Psi_1^{S\dagger}(i\sigma\sigma') = \frac{1}{\sqrt{2}}\left(c^\dagger_{i1\sigma}c^\dagger_{i2\sigma'} - c^\dagger_{i1\sigma'}c^\dagger_{i2\sigma}\right), \quad (11)$$
$$\Psi_2^{S\dagger}(i\sigma\sigma') = c^\dagger_{i1\sigma}c^\dagger_{i1\sigma'}, \quad (12)$$
$$\Psi_3^{S\dagger}(i\sigma\sigma') = c^\dagger_{i2\sigma}c^\dagger_{i2\sigma'}. \quad (13)$$

The perturbative component to the Hamiltonian includes a Ni-Ni nearest neighbor hopping term ($H_{\rm tun}$)

Racah A[a]	6.6eV	$(pd\sigma)^a$	1.3eV
Racah B[a]	0.13eV	$(pd\pi)^a$	-0.6eV
Racah C[a]	0.60eV	$\langle r^2 \rangle^b$	0.27 Å^2
$\Delta^{a,c}$	6.2eV	$\langle r^4 \rangle^b$	0.16 Å^4
λ	0.020eV		

TABLE III: Model Parameters
[a] Data for NiO doped with Li.[27]
[b] Determined using the radial wave function from a Roothaan-Hartree-Fock calculation.[28]
[c] Defined as the energy to move an electron from an O atom in a 2p state to a Ni atom in a 3d state.

t^{12}, t^{14}	t^{13}
$\begin{pmatrix} -0.0336 & 0.0609 \\ 0.0609 & 0.0648 \end{pmatrix}$	$\begin{pmatrix} -0.0821 & 0.0000 \\ 0.0000 & 0.0320 \end{pmatrix}$

TABLE IV: Hopping matrix elements $t^{ij}_{\alpha\beta}$ in units of eV. From Fig. 1 we see that there are three distinct hopping paths between neighboring Ni ions, the path between 1 and 2, the path between 1 and 3, and the path between 1 and 4.

which moves an electron from one Ni site to a neighboring site, and a spin-orbit coupling term ($H_{\rm SO}$). The spin orbit interaction connects the Hamiltonian to the lattice and is responsible for the anisotropic part of the exchange ($\mathbf{A}_{ij}$). The spin orbit term is given by

$$H_{\rm SO} = \frac{\lambda}{2} \sum_{\substack{i\alpha\beta \\ \sigma\sigma'}} \sum_{\substack{\mu= \\ x,y,z}} \langle i\alpha | L_\mu | i\beta \rangle \hat{\sigma}^\mu_{\sigma\sigma'} c^\dagger_{i\alpha\sigma} c_{i\beta\sigma'},$$

where $\langle i\alpha | L | i\beta \rangle$ is the orbital matrix element between crystal field states and $\hat{\sigma}^\mu$ are Pauli spin matrices.

The tunneling Hamiltonian is given by:

$$H_{\rm tun} = \sum_{\substack{ij\alpha\beta \\ \sigma}} t^{ij}_{\alpha\beta} c^\dagger_{i\alpha\sigma} c_{j\beta\sigma} + h.c. \tag{14}$$

where $t^{ij}_{\alpha\beta}$ is an effective hopping between Ni ions i and j whose values are given in Table IV. There are two principle hopping paths which connect neighboring Ni ions, each via a neighboring O ion, as shown in Fig. 1. The two paths are included in the effective hopping element $t^{ij}_{\alpha\beta}$ in the following manner:

$$t^{ij}_{\alpha\beta} = -\frac{1}{\Delta} \sum_{ka} t^{ik}_{\alpha a} t^{jk}_{\beta a}, \tag{15}$$

where $t^{ik}_{\alpha a}$ hops an electron from the p orbital a on the O ion k to the e_g orbital α on the Ni ion i. The value of $t^{ik}_{\alpha a}$ is determined from the Slater Koster integrals, $(pd\sigma)$ and $(pd\pi)$,[29] whose values, along with all the other parameters used in the calculation, are listed in Table III.

J_{12}, J_{14}	J_{13}
-0.0812	0.0000
A_{12}, A_{14}	A_{13}
$\begin{pmatrix} 0.2031 & 0.0000 & 0.1041 \\ 0.0000 & 0.0593 & 0.0000 \\ 0.1041 & 0.0000 & 0.1346 \end{pmatrix}$	$\begin{pmatrix} -0.0629 & 0.0000 & 0.0064 \\ 0.0000 & -0.0715 & 0.0000 \\ 0.0064 & 0.0000 & -0.0669 \end{pmatrix}$

TABLE V: Coupling constants, in units of meV, determined from perturbation theory.

Using resolvent perturbation theory[30] (see Appendix B) the lowest order contribution to the exchange couplings comes from a term which is zeroth order in λ and second order in t and, as such, affects only the isotropic exchange couplings (J_{ij}). The term of order λt^2 contributes only to the antisymmetric exchange which is zero due to the presence of inversion centers at the center of each Ni-Ni nearest neighbor bond. The term of order $\lambda^2 t^2$ contributes to the symmetric exchange $\mathbf{A}_{ij}$. Results are shown in Table V.

The exchange anisotropy can be diagonalized by rotating the system through 54° around the y-axis. The eigenvalues of $\mathbf{A}_{12}$ and $\mathbf{A}_{14}$ are 0.2785 meV, 0.0593 meV, and 0.0593 meV while the eigenvalues of $\mathbf{A}_{13}$ are -0.05816 meV, -0.0715 meV and -0.0715 meV.

III. SPIN WAVE SPECTRUM

The simplest Hamiltonian consistent with the calculation of the anisotropic spin couplings is given by

$$H = \sum_{\langle ij \rangle_\perp} J^\perp_{ij} \mathbf{S}_i \cdot \mathbf{S}_j + \sum_{\langle ij \rangle_\parallel} J^\parallel_{ij} \mathbf{S}_i \cdot \mathbf{S}_j + \sum_{\langle ij \rangle_\parallel} K^{xx}_{ij} S^x_i S^x_j \tag{16}$$

where $\langle ij \rangle_\perp$ ($\langle ij \rangle_\parallel$) indicates the sum is over interplane (in-plane) nearest neighbors, $J^\perp_{ij}$ is the interplane coupling, $J^\parallel_{ij}$ is the in-plane coupling and K^{xx}_{ij} is the easy plane anisotropy determined in Sec. II. For notational simplicity the anisotropic interaction is decomposed into two parts, an isotropic component included in $J^\perp_{ij}$ and an easy plane anisotropic component labeled K^{xx}_{ij}. Hence, for Ni-Ni bonds of the type between Ni ions 1 and 2 in Fig. 1 we have $K^{xx}_{ij} = K_1 = 0.2192$ meV. Similarly, the bonds between ions such as 1 and 3 have $K^{xx}_{ij} = K_2 = 0.0135$ meV and between 1 and 4 have $K^{xx}_{ij} = K_3 = 0.2192$ meV. The coordinate system has been chosen so that the yz plane makes an angle of 54° with the NiO plane.

In this section it is assumed that $J^\parallel_{ij} = J^\parallel$ and $J^\perp_{ij} = J^\perp$, however other possibilities are discussed in Sec. V. The goal of this section is to determine the spin wave dispersion in the linear spin wave approximation.

As discussed in Sec. I, the interplane exchange should be antiferromagnetic, hence the Néel state is described by a two sublattice (denoted A and B) model: all spins on a given NiO plane are aligned while spins on neighboring NiO planes are antiparallel.

In linear spin wave theory the Holstein Primakoff transformation for the spin operators on sublattice A is given by:

$$\begin{aligned} S^x_{\mathbf{r}_A} &= \sqrt{\tfrac{S}{2}}\left(a^\dagger_{\mathbf{r}} + a_{\mathbf{r}}\right), \\ S^y_{\mathbf{r}_A} &= i\sqrt{\tfrac{S}{2}}\left(a^\dagger_{\mathbf{r}} - a_{\mathbf{r}}\right), \\ S^z_{\mathbf{r}_A} &= S - a^\dagger_{\mathbf{r}} a_{\mathbf{r}}, \end{aligned} \tag{17}$$

where $a^\dagger_{\mathbf{r}}$ ($a_{\mathbf{r}}$) creates (annihilates) a boson on site $\mathbf{r}$. The bosonic representation for the spins on sublattice B is found by performing a rotation of 180° about the x-axis:

$$\begin{aligned} S^x_{\mathbf{r}_B} &= \sqrt{\tfrac{S}{2}}\left(b^\dagger_{\mathbf{r}} + b_{\mathbf{r}}\right), \\ S^y_{\mathbf{r}_B} &= -i\sqrt{\tfrac{S}{2}}\left(b^\dagger_{\mathbf{r}} - b_{\mathbf{r}}\right), \\ S^z_{\mathbf{r}_B} &= -S + b^\dagger_{\mathbf{r}} b_{\mathbf{r}}. \end{aligned} \tag{18}$$

Within linear spin wave theory, only terms quadratic in bosonic operators are kept. Taking the Fourier transform of the resulting Hamiltonian gives:

$$H_2 = \sum_{\mathbf{k}} \gamma^\dagger_{\mathbf{k}} \mathbf{H}\left(\mathbf{k}\right) \gamma_{\mathbf{k}}, \tag{19}$$

where

$$\gamma^\dagger_{\mathbf{k}} = \left[a^\dagger_{\mathbf{k}} \;\; b^\dagger_{-\mathbf{k}} \;\; a_{-\mathbf{k}} \;\; b_{\mathbf{k}}\right], \tag{20}$$

and

$$\mathbf{H}\left(\mathbf{k}\right) = \begin{bmatrix} A_{\mathbf{k}} & D_{\mathbf{k}} & C_{\mathbf{k}} & B_{\mathbf{k}} \\ D_{\mathbf{k}} & A_{\mathbf{k}} & B_{\mathbf{k}} & C_{\mathbf{k}} \\ C_{\mathbf{k}} & B_{\mathbf{k}} & A_{\mathbf{k}} & D_{\mathbf{k}} \\ B_{\mathbf{k}} & C_{\mathbf{k}} & D_{\mathbf{k}} & A_{\mathbf{k}} \end{bmatrix}, \tag{21}$$

with

$$\begin{aligned} A_{\mathbf{k}} &= 2J^{\parallel} S \sum_{j=1}^{3} \left(\cos\left(\mathbf{k}\cdot\mathbf{t}_j\right) - 1\right) \\ &\quad + 6J^{\perp} S + S\sum_{j=1}^{3} K_j \cos\left(\mathbf{k}\cdot\mathbf{t}_j\right), \end{aligned} \tag{22}$$

$$B_{\mathbf{k}} = 2J^{\perp} S \sum_{j=1}^{3} \cos\left(\mathbf{k}\cdot\mathbf{u}_j\right), \tag{23}$$

$$C_{\mathbf{k}} = S\sum_{j=1}^{3} K_j \cos\left(\mathbf{k}\cdot\mathbf{t}_j\right), \tag{24}$$

$$D_{\mathbf{k}} = 0. \tag{25}$$

The nearest neighbor vectors in the NiO planes have been denoted $\pm\mathbf{t}_j$, while the nearest neighbor vectors between planes are $\pm\mathbf{u}_j$.

Equation (19) is diagonalized by solving the eigenequation[31]

$$\eta\mathbf{H}\left(\mathbf{k}\right) T_{\mathbf{k}} = T_{\mathbf{k}} \eta \Omega_{\mathbf{k}}. \tag{26}$$

where $T_{\mathbf{k}}$ is the linear transformation defined by $\boldsymbol{\gamma}_{\mathbf{k}} = T_{\mathbf{k}}\boldsymbol{\xi}_{\mathbf{k}}$, $\Omega_{\mathbf{k}}$ is a matrix containing the eigenvalues, and $\eta = \left[\boldsymbol{\gamma}_{\mathbf{k}}, \boldsymbol{\gamma}^\dagger_{\mathbf{k}}\right] = \left[\boldsymbol{\xi}_{\mathbf{k}}, \boldsymbol{\xi}^\dagger_{\mathbf{k}}\right]$.

Solving Eq. 26, the linear transformation $T_{\mathbf{k}}$ is given by

$$T_{\mathbf{k}} = \begin{bmatrix} u_1\left(\mathbf{k}\right) & v_1\left(\mathbf{k}\right) & u_2\left(\mathbf{k}\right) & v_2\left(\mathbf{k}\right) \\ -u_1\left(\mathbf{k}\right) & v_1\left(\mathbf{k}\right) & -u_2\left(\mathbf{k}\right) & v_2\left(\mathbf{k}\right) \\ u_2\left(\mathbf{k}\right) & v_2\left(\mathbf{k}\right) & u_1\left(\mathbf{k}\right) & v_1\left(\mathbf{k}\right) \\ -u_2\left(\mathbf{k}\right) & v_2\left(\mathbf{k}\right) & -u_1\left(\mathbf{k}\right) & v_1\left(\mathbf{k}\right) \end{bmatrix}$$

where

$$\begin{aligned} u_{\left(\frac{1}{2}\right)}\left(\mathbf{k}\right) &= -\frac{1}{2}\sqrt{\frac{A_{\mathbf{k}} - D_{\mathbf{k}} \pm \omega_1\left(\mathbf{k}\right)}{\omega_1\left(\mathbf{k}\right)}}, \\ v_{\left(\frac{1}{2}\right)}\left(\mathbf{k}\right) &= \mp\frac{1}{2}\sqrt{\frac{A_{\mathbf{k}} + D_{\mathbf{k}} \pm \omega_2\left(\mathbf{k}\right)}{\omega_2\left(\mathbf{k}\right)}}. \end{aligned} \tag{27}$$

The dispersion relations, $\omega_1(\mathbf{k})$ and $\omega_2(\mathbf{k})$, are given by

$$\omega_{\left(\frac{1}{2}\right)}\left(\mathbf{k}\right) = \sqrt{\left(A_{\mathbf{k}} \mp D_{\mathbf{k}}\right)^2 - \left(B_{\mathbf{k}} \mp C_{\mathbf{k}}\right)^2}. \tag{28}$$

Hence the harmonic Hamiltonian is

$$H_2 = \sum_{\mathbf{k}} \left[\omega_1\left(\mathbf{k}\right)\alpha^\dagger_{\mathbf{k}}\alpha_{\mathbf{k}} + \omega_2\left(\mathbf{k}\right)\beta^\dagger_{\mathbf{k}}\beta_{\mathbf{k}}\right]. \tag{29}$$

Comparing this result with the inelastic neutron scattering data (see Fig. 3(a))[19] and using the values for the anisotropic coupling constants K_{ij} determined in Sec. II, we can ascertain the coupling constants $J^{\parallel}$ and $J^{\perp}$ associated with the model (Eq. (16)). Since the ferromagnetic in-plane coupling is approximately ten times larger than the antiferromagnetic interplane couplings,[12] the spin wave dispersion seen in Fig. 3(a) is due mostly to the antiferromagnetic exchange. When $\mathbf{k}$ is perpendicular to the ferromagnetic planes, the ferromagnetic contribution to the magnon energies is zero. Hence, matching the zone boundary spin wave energy along $\mathbf{k}$ perpendicular to the NiO planes,

$$\Delta_{max} = 6S\sqrt{(J^{\perp})^2 + \frac{1}{3}J^{\perp}\sum_j K_j}, \tag{30}$$

to the zone boundary spin wave energy (approximately 0.7 meV) in Fig. 3(a), we find $J^{\perp} = 0.17$ meV. The

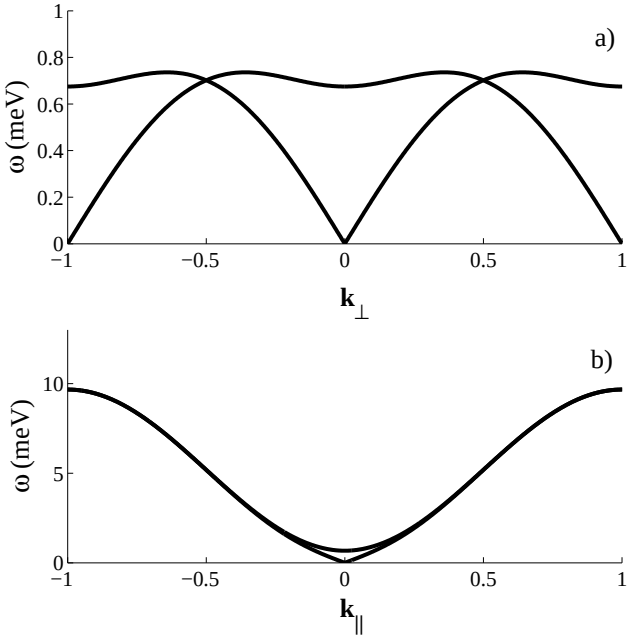

FIG. 2: Spin-wave dispersions. In (a), $\mathbf{k}$ is perpendicular to the NiO planes and scaled so that 1 corresponds to the Brioullin zone boundary (π/c). In (b) $\mathbf{k}$ is in a nearest neighbor direction in the NiO plane and scaled to the ferromagnetic Brioullin zone boundary ($2\pi/\sqrt{3}$a).

Curie-Weiss temperature (Θ) relates the three couplings:

$$\Theta = -\frac{6}{k_B}\left(\frac{S\left(S+1\right)}{9}\right)\left(3J^{\perp}+3J^{\parallel}+\frac{1}{3}\sum_j K_j\right). \tag{31}$$

Using $\Theta = 36$ K[12] we find $J^{\parallel} = -2.29$ meV. These results are consistent with the results reported in Ref. 12.

In Fig. 2, the dispersion curves are plotted along the wavevector $\mathbf{k}$ perpendicular to the NiO plane and along a reciprocal lattice vector in the triangular plane. In Figs. 2(a) and (b) the dispersion curves for the acoustic mode are linear in the low $\mathbf{k}$ limit as expected for an antiferromagnet with Néel order. In contrast, ferromagnets display quadratic behavior in the small $\mathbf{k}$ limit. In Fig. 2(b), the ferromagnetic interaction quickly dominates the dispersion as $\mathbf{k}$ increases. Interestingly, however, despite the dominating strength of the ferromagnetic interaction, there does not exist a direction in which the behavior of the acoustic dispersion curve is quadratic as $\mathbf{k}$ approaches zero. The spins which couple antiferromagnetically in the model have nearest neighbors in all three dimensions so the antiferromagnetic coupling always contributes to the dispersion. In contrast, in the direction perpendicular to the NiO planes, there is no nearest neighbor ferromagnetic interaction which contributes to the dispersion. Thus, the behavior at low energies is dominated by dispersion along $\mathbf{k}$ corresponding to vectors which are approximately perpendicular to the ferromagnetic planes, justifying the method used to determine $J^{\perp}$.

The optical mode seen in Fig. 2(a) is flat on the 1 meV energy scale. We argue below that it gives rise to the dispersionless scattering seen at 0.7 meV in Fig. 3(a).

IV. INELASTIC NEUTRON CROSS SECTION

The inelastic neutron scattering cross section is given by

$$\frac{d^2\sigma}{d\Omega dE'}\left(\boldsymbol{\kappa},\omega\right) \propto \frac{k'}{k}\sum_{\alpha,\beta}\left(\delta_{\alpha,\beta}-\hat{\boldsymbol{\kappa}}_\alpha\hat{\boldsymbol{\kappa}}_\beta\right)\times \sum_{\mathbf{R}\mathbf{R}'} e^{-i\boldsymbol{\kappa}\cdot\left(\mathbf{R}-\mathbf{R}'\right)}\int_{-\infty}^{\infty} dt e^{-i\omega t}\left\langle S^{\alpha}_{\mathbf{R}}\left(0\right)S^{\beta}_{\mathbf{R}'}\left(t\right)\right\rangle, \tag{32}$$

where $\boldsymbol{\kappa} = \mathbf{k}'-\mathbf{k}$, $\mathbf{k}$ ($\mathbf{k}'$) is the momentum of the incoming (outgoing) neutron. The Fourier transforms of the spin-spin correlation functions are evaluated in Appendix C and the result yeilds:

$$\frac{d^2\sigma}{d\Omega dE'}\left(\boldsymbol{\kappa},\omega\right) \propto \frac{k'}{k}\frac{S}{2}\left(1+\eta\left(\omega\right)\right)\int\frac{d^3q}{\left(2\pi\right)^3}\sum_{\boldsymbol{\tau}\alpha}\left[\delta\left(\omega-\omega_\alpha\left(\mathbf{q}\right)\right)\delta\left(\boldsymbol{\kappa}-\mathbf{q}+\boldsymbol{\tau}\right)+\delta\left(\omega+\omega_\alpha\left(\mathbf{q}\right)\right)\delta\left(\boldsymbol{\kappa}+\mathbf{q}+\boldsymbol{\tau}\right)\right]\times$$
$$\left[\left(1+\hat{\boldsymbol{\kappa}}_z^2\right)\left(\left(\Psi_1^\alpha\right)^2+\left(\Psi_2^\alpha\right)^2+2\Psi_1^\alpha\Psi_2^\alpha\cos\left(\boldsymbol{\rho}\cdot\boldsymbol{\tau}\right)\right)+\left(-1\right)^\alpha\left(\hat{\boldsymbol{\kappa}}_y^2+\hat{\boldsymbol{\kappa}}_x^2\right)\left(\left(\left(\Psi_1^\alpha\right)^2+\left(\Psi_2^\alpha\right)^2\right)\cos\left(\boldsymbol{\rho}\cdot\boldsymbol{\tau}\right)+2\Psi_1^\alpha\Psi_2^\alpha\right)\right] \tag{33}$$

where $\Psi^1 = [u_1, -u_2]$ and $\Psi^2 = [v_1, v_2]$ are defined to simplify the expression, $\boldsymbol{\rho}$ is a vector between nearest neighbor Ni ions on different sublattices (ie. $\boldsymbol{\rho} = \mathbf{u}_1$) and $\eta(\omega) = \left(e^{\omega/kT}+1\right)^{-1}$ is the Bose distribution function.

For a powder sample, as is the case of Fig. 3(a), one measures

$$D\left(\kappa,\omega\right) = \int d\Omega_{\boldsymbol{\kappa}}\ \frac{d^2\sigma}{d\Omega dE'}, \tag{34}$$

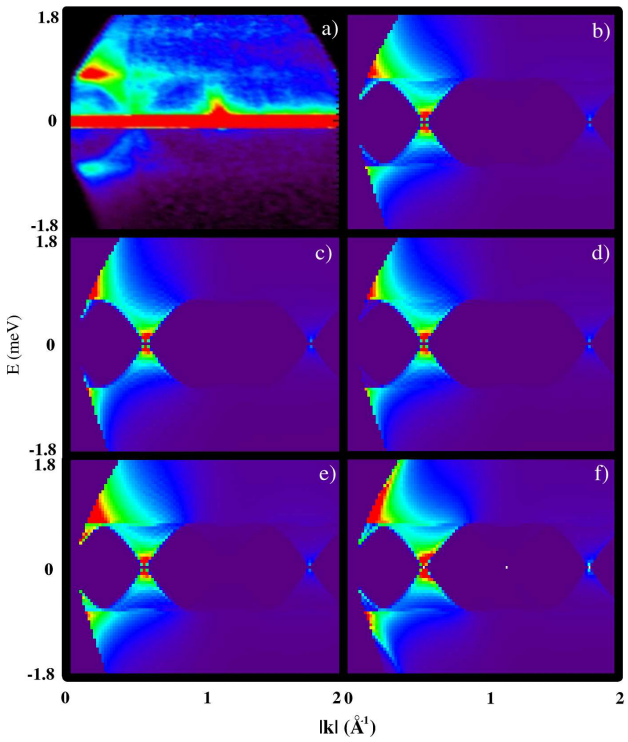

FIG. 3: Experimental and theoretical plots of the inelastic neutron scattering cross section on a powder sample of $NaNiO_2$ at 10K. The experimental data from measurements at NIST is shown in (a).[19] In (b) the inelastic neutron cross section resulting from the theoretical results is displayed where the isotropic spin couplings are assumed to be equal for all in-plane and interplane nearest neighbor bonds, specifically $J_{ij}^{\perp} = J^{\perp}$ and $J_{ij}^{\parallel} = J^{\parallel}$. The angle between the NiO planes and the easy spin plane is 54°. In (c), (d) and (e) we contrast (b) with plots where the angle the easy spin plane makes with NiO planes is varied; the angles are 0°, 30° and 90° respectively. In (f) it is assumed that $J_{ij}^{\perp} = J^{\perp}$ and $J_{12}^{\parallel} = J_{14}^{\parallel} = 10 J_{13}^{\parallel}$, and the angle between the easy spin plane and the NiO plane is again 54°.

where $\Omega_{\boldsymbol{\kappa}}$ is the solid angle associated with $\boldsymbol{\kappa}$. To express this integral in Cartesian coordinates, note that

$$\int d\Omega_{\boldsymbol{\kappa}'} \;\rightarrow\; \int d\boldsymbol{\kappa}' \frac{1}{\kappa^2} \delta\left(\kappa - \kappa'\right). \tag{35}$$

Using the integral representation given by Eq. (35) we evaluate Eq.(34) numerically. To perform the integral over the delta functions numerically, we note that for each value of $\boldsymbol{\kappa}$ there exists a unique $\omega_1(\boldsymbol{\kappa})$ and $\omega_2(\boldsymbol{\kappa})$. The weights associated with each value of $\boldsymbol{\kappa}$ are binned according to both κ and the corresponding $\omega_j(\mathbf{q})$, where $j = 1, 2$ and $\mathbf{q}$ satisfies the expression $(\boldsymbol{\kappa} \mp \mathbf{q} - \boldsymbol{\tau}) = 0$ for a reciprocal lattice vector $\boldsymbol{\tau}$. For a given $\boldsymbol{\kappa}$ there is only one choice of $\mathbf{q}$ and $\boldsymbol{\tau}$ that satisfy this equation. This statement follows from the observation that since $\boldsymbol{\tau}$ is a reciprocal lattice vector and $\mathbf{q}$ is restricted to lie inside the first Brillouin zone, a general vector can be decomposed uniquely into a $\boldsymbol{\tau}$ and $\mathbf{q}$. The size of the κ bins and ω bins has been chosen such that the intensity profile does not change as the size of the bins decreases. We have found that using $\Delta\kappa = 0.004$ Å^{-1} and $\Delta\omega = 0.05$ meV is sufficient.

Figures. 3 (b), (c), (d) and (e) show $D(\kappa, \omega)$ with the exchange couplings determined in Sec. II for various angles between the NiO plane and the easy plane. In the experimental plot, Fig. 3(a), two modes are clearly visible: a Goldstone mode which goes to zero near 0.6 Å^{-1} and a dispersionless mode near 0.7 meV. In all theoretical plots the Goldstone mode is clearly visible. However, as the angle between the easy spin plane and the NiO plane is varied, the weight of the dispersionless mode changes dramatically. The best agreement between theory and experiment is found for an angle near 54°, as shown in Fig. 3(b).

V. DISCUSSION

Our analysis of the crystal fields, Coulomb interactions, spin-orbit couplings, and tunneling terms appropriate for $NaNiO_2$ has led to a simple anisotropic exchange Hamiltonian which gives a remarkably good description of the magnetic behavior observed in this material. Our point charge calculation of the Ni^{3+} d-orbital ground state shows the t_{2g}-e_g splitting expected in $NaNiO_2$. Using this orbital ordering, we find the spin-orbit contribution to the anisotropy in the in-plane Ni-O-Ni superexchange corresponds to easy plane anisotropy where the easy plane makes an angle of 54° with the NiO planes. This kind of anisotropy was inserted by Lewis *et al.*,[19] but without any microscopic motivation. Our calculations provide that motivation. In addition, the resulting isotropic interactions, found by comparing our model to inelastic neutron scattering measurements and the Curie-Weiss temperature, are similar to those reported by Chappel *et al.*[12] and Lewis *et al.*[19]: the isotropic ferromagnetic in-plane interaction is approximately ten times larger than the isotropic antiferromagnetic interplane coupling. The corresponding theoretical inelastic neutron scattering cross section clearly displays both the Goldstone and dispersionless modes seen experimentally. As noted by Lewis *et al.*,[19] the dispersionless mode is only seen when the angle between the NiO plane and the easy spin plane is nonzero. The calculated value of 54° is in good agreement with experiment.

As mentioned in Sec. III, we have made a significant simplification to study this system by assuming that $J_{ij}^{\perp}$ and $J_{ij}^{\parallel}$ are independent of i and j. From the perturbative calculation in Sec. II we note that there are two different Ni-Ni nearest neighbor bonds in the NiO planes: in Fig. 1 the bonds between Ni ions 1 and 2, and 1 and 4 are the same, while the bond between 1 and 3 gives a substantially different result (see the tunneling data in Table IV). It would be reasonable to assume this to

be true for the $J_{ij}^{\parallel}$ exchange integral as well. Unfortunately, however, there is not yet sufficient experimental data to distinguish between the two bonds. For example, in Fig. 3(f), we show the neutron scattering cross section for $J_{12}^{\parallel} = J_{14}^{\parallel} = 10J_{13}^{\parallel} = J^{\parallel}$. This result is also consistent with experiment. However, based on the current experimental data, including neutron scattering measurements[19] magnetization and magnetic susceptibility measurements,[12] it is impossible to exactly determine the isotropic spin couplings. However, the calculation does indicate that the nearest neighbor in-plane interactions are ferromagnetic, as one would expect from the Goodenough rules and in contradiction to the magnetic structure proposed by Vernay *et al.*[9]

Given our success in explaining the observed magnetic ordering in $NaNiO_2$, it is interesting to speculate about the implications our results may have on the anomalous magnetic behavior in $LiNiO_2$. First we note that similar calculations for $LiNiO_2$ would not be possible for two reasons. First, the ordering of the Ni d-oribtals in $LiNiO_2$ is not known. There is no long range order, but there may be sufficient short range order which would affect calculations of magnetic interactions. Second, the determination of $J^{\perp}$ relies on spin wave data for the magnetically ordered state in $NaNiO_2$. Since $LiNiO_2$ does not order, it is not clear how to determine $J^{\perp}$. However, while our calculations are specific to the long range orbital ordering present in $NaNiO_2$, the similarities between the high temperature structures and the ferromagnetic Curie-Weiss temperatures of both materials, suggest that the exchange couplings should be similar and, specifically, that the exchange couplings in the NiO layers of $LiNiO_2$ are ferromagnetic. This is incompatible with proposals based on frustrated triangular layers,[10,11] but would be compatible with proposals based on disorder due to some Ni ions at the alkali metal sites.[13,19] While Li ions have an atomic radius approximately equal to the radius of Ni (∼0.7 Å), the Na ion radius is significantly larger (∼1 Å) and hence the lighter Li ions are more prone to this type of site disorder than the Na ions. Consequently, this disorder would be expected to play a more significant role in the magnetic behavior of $LiNiO_2$. This disorder introduces extra exchange paths between the magnetic site impurities and the neighboring Ni planes. Since the interplane coupling is antiferromagnetic, regardless of whether the new exchange interactions are ferromagnetic or antiferromagnetic, a new interlayer site introduces frustrated interactions. As noted by Lewis *et al.*[19] and Chappel *et al.*,[13] this induced frustration could then produce the anomalous spin glass behavior seen in $LiNiO_2$.

VI. ACKNOWLEDGMENTS

The authors acknowledge useful discussions with Brooks Harris, Bruce Gaulin, Patrick Clancy and Mike Lewis. Financial support from NSERC and the Canadian Institute for Advanced Research is also acknowledged.

APPENDIX A: STATIC CRYSTAL FIELD HAMILTONIAN

In this section we determine the static crystal field eigenorbitals and energies. Treating each ion in the crystal as a point charge, the Coulomb sum gives the following contribution to the Hamiltonian

$$H(\mathbf{r}) = \frac{q(\mathbf{r})}{4\pi\epsilon_0} \sum_{\mathbf{R}} \frac{q(\mathbf{R})}{|\mathbf{r}-\mathbf{R}|} \tag{A1}$$

where $q(\mathbf{R}) = 3, -2, 1$ for Ni^{3+}, O^{2-} and Na^{1+}, respectively. Using the transformation

$$\frac{1}{|\mathbf{r}-\mathbf{R}|} = \sum_{l=0}^{\infty} \sum_{m=-l}^{l} \frac{r^l}{R^{l+1}} \frac{4\pi}{2l+1} Y_{l,m}^{*}(\Theta,\Phi)\, Y_{l,m}(\theta,\phi) \tag{A2}$$

where $\mathbf{r} = (r,\theta,\phi)$ and $\mathbf{R} = (R,\Theta,\Phi)$ the matrix elements become:

$$\begin{aligned}
&\left\langle 2,m'\right| H(\mathbf{r}) \left|2,m''\right\rangle \\
&\quad = \frac{q(\mathbf{r})}{4\pi\epsilon_0} \sum_{\mathbf{R}} \sum_{l=0}^{\infty} \sum_{m=-l}^{l} q(\mathbf{R}) \frac{4\pi(-1)^{m'+m}}{2l+1} \frac{Y_{l,-m}(\Theta,\Phi)}{R^{l+1}} \int d^3r\, r^l Y_{2,-m'}(\theta,\phi)\, Y_{l,m}(\theta,\phi)\, Y_{2,m''}(\theta,\phi) \\
&\quad = \frac{q(\mathbf{r})}{4\pi\epsilon_0} \sum_{\substack{l=\\0,2,4}} \sum_{m=-l}^{l} (-1)^{m'+m} \sqrt{\frac{100\pi}{2l+1}} \langle r^l \rangle \begin{pmatrix} 2 & l & 2 \\ 0 & 0 & 0 \end{pmatrix} \begin{pmatrix} 2 & l & 2 \\ -m' & m & m'' \end{pmatrix} \sum_{\mathbf{R}} q(\mathbf{R}) \frac{Y_{l,-m}(\Theta,\Phi)}{R^{l+1}}.
\end{aligned} \tag{A3}$$

The restriction on the l-sum comes from the zeros of the Wigner 3-j symbols. The radial wavefunction is determined in Ref. 28 by the Roothaan-Hartree-Fock method and gives $\langle r^2 \rangle$ =0.27 Å^2 and $\langle r^4 \rangle$ =0.16 Å^4.

m', m''	-2	-1	0	1	2
-2	-0.0352	0.1290	0.0577	0.0000	-0.0126
-1	0.1290	0.0751	0.0527	0.1128	-0.0000
0	0.0577	0.0527	-0.0798	-0.0527	0.0577
1	0.0000	0.1128	-0.0527	0.0751	-0.1290
2	-0.0126	-0.0000	0.0577	-0.1290	-0.0352

TABLE VI: Matrix elements $\langle 2, m'|H(\mathbf{r})|2, m''\rangle$ where $\mathbf{r}$ is any Ni site, in eV.

The $l = 0$ term corresponds to a monopole sum over a neutral crystal which can be evaluated using the Ewald summation technique. However, it only contributes to an overall energy shift and not to the energy splittings hence we do not include it here. The $l = 2$ term can be evaluated by noting that the spherical harmonics can be written in terms of $Q_{i,j} = \left(3\mathbf{x}_i\mathbf{x}_j - R^2\delta_{i,j}\right)/R^2$. The sum $\sum_{\mathbf{R}} Q_{i,j}/R^3$ is a dipole Ewald sum evaluated when $\mathbf{q} = 0$. A complete description of the Ewald summation in the case of a dipolar interaction is found in Ref. 32. The $l = 4$ (quadrapole) term converges quickly and can be evaluated by a straight forward numerical sum. The resulting matrix elements, $\langle 2, m'|H(\mathbf{r})|2, m''\rangle$ for Ni ions are given in Table VI. The resulting eigenenergies and eigenvalues in terms of the cubic crystal field states are shown in Table II.

APPENDIX B: PERTURBATION THEORY

The perturbation theory calculation we use to determine the anisotropic spin couplings is based on the calculation of Schmit *et al.*[20] To start, we define the following projection operators:

$$P_0^{ij} = \sum_{\sigma,\sigma'} c^\dagger_{i0\sigma} c^\dagger_{j0\sigma'} |0\rangle\langle 0| c_{j0\sigma'} c_{i0\sigma}, \tag{B1}$$

which projects onto the ground state,

$$P_1^{ij} = \sum_{\substack{\sigma,\sigma' \\ \alpha\beta\neq 00}} c^\dagger_{i\alpha\sigma} c^\dagger_{j\beta\sigma'} |0\rangle\langle 0| c_{j\beta\sigma'} c_{i\alpha\sigma}, \tag{B2}$$

which projects onto the Ni^{3+} sector, and

$$P_2^{ij} = \frac{1}{2}\sum_{k\sigma\sigma'} \Big[\Psi_1^{T\dagger}(k\sigma\sigma')|0\rangle\langle 0|\Psi_1^T(k\sigma\sigma') + \sum_{\nu=1}^{3} \Psi_\nu^{S\dagger}(k\sigma\sigma')|0\rangle\langle 0|\Psi_\nu^S(k\sigma\sigma')\Big], \tag{B3}$$

which projects onto the Ni^{2+} sector.

The resolvent operators are then given by the following:

$$S_1^{ij} = \frac{1}{\Delta E} P_1^{ij} = -\sum_{\substack{\sigma,\sigma' \\ \alpha\beta\neq 00}} \frac{1}{E_\alpha + E_\beta} c^\dagger_{i\alpha\sigma} c^\dagger_{j\beta\sigma'} |0\rangle\langle 0| c_{j\beta\sigma'} c_{i\alpha\sigma}, \tag{B4}$$

$$S_2^{ij} = \frac{1}{\Delta E} P_2^{ij} = -\frac{1}{2}\sum_{\substack{k \\ \sigma\sigma'}} \Bigg[\frac{1}{E_T}\Psi_1^{T\dagger}(k\sigma\sigma')|0\rangle\langle 0|\Psi_1^T(k\sigma\sigma') + \sum_{\substack{\nu_1 \\ \nu\nu'}} \frac{M^k_{\nu\nu_1} M^k_{\nu_1\nu'}}{E^S_{\nu_1}} \Psi_{\nu'}^{S\dagger}(k\sigma\sigma')|0\rangle\langle 0|\Psi_\nu^S(k\sigma\sigma')\Bigg], \tag{B5}$$

where the matrix M diagonalizes the spin singlet sector of $H_{CF} + H_C$ and E_S^ν are the corresponding energies.

Expanding in terms of the spin orbit coupling, the zeroth order term is given by:

$$J_{ij}^{(1)} \mathbf{S}_i \cdot \mathbf{S}_j = P_0^{ij} H_{\rm tun}^{ij} S_2^{ij} H_{\rm tun}^{ij} P_0^{ij}. \tag{B6}$$

Since this term does not connect to the lattice in any way, it can only contribute to the isotropic coupling. The term first order in spin orbit coupling only contributes to the antisymmetric exchange and thus is zero for $NaNiO_2$. The second order term contributes to symmetric anisotropic couplings (such as $\mathbf{A}_{ij}$) as well as to the isotropic couplings. It is given by:

$$\begin{aligned} J_{ij}^{(2)} \mathbf{S}_i \cdot \mathbf{S}_j + \mathbf{S}_i \mathbf{A}_{ij} \mathbf{S}_j &= P_0^{ij} H_{\rm SO}^{ij} S_1^{ij} H_{\rm SO}^{ij} S_1^{ij} H_{\rm tun}^{ij} S_2^{ij} H_{\rm tun}^{ij} P_0^{ij} \\ &+ P_0^{ij} H_{\rm SO}^{ij} S_1^{ij} H_{\rm tun}^{ij} S_2^{ij} H_{\rm tun}^{ij} S_1^{ij} H_{\rm SO}^{ij} P_0^{ij} \\ &+ P_0^{ij} H_{\rm tun}^{ij} S_2^{ij} H_{\rm tun}^{ij} S_1^{ij} H_{\rm SO}^{ij} S_1^{ij} H_{\rm SO}^{ij} P_0^{ij} \\ &- \frac{1}{2} P_0^{ij} H_{\rm SO}^{ij} S_1^{ij} S_1^{ij} H_{\rm SO}^{ij} P_0^{ij} H_{\rm tun}^{ij} S_2^{ij} H_{\rm tun}^{ij} P_0^{ij} \\ &- \frac{1}{2} P_0^{ij} H_{\rm tun}^{ij} S_2^{ij} H_{\rm tun}^{ij} P_0^{ij} H_{\rm SO}^{ij} S_1^{ij} S_1^{ij} H_{\rm SO}^{ij} P_0^{ij} \end{aligned} \tag{B7}$$

where we have omitted terms where S_2^{ij} appears twice. The energy denominator of S_1^{ij} goes like the crystal field energy E_1 while the characteristic energy for S_2^{ij} comes from a combination of the crystal field energy and the much larger Coulomb energy. The omitted terms are thus at least a factor of ten smaller than those kept.

The creation and annihilation operators which occur when evaluating Eqs. B5 and B7 can be converted to spin operators using the following relations:

$$c^\dagger_{i0\uparrow} c_{i0\downarrow} = S_i^+, \tag{B8}$$

$$c^\dagger_{i0\downarrow} c_{i0\uparrow} = S_i^-, \tag{B9}$$

$$c^\dagger_{i0\uparrow} c_{i0\uparrow} = S_i^z + \frac{1}{2}, \tag{B10}$$

$$c^\dagger_{i0\downarrow} c_{i0\downarrow} = -S_i^z + \frac{1}{2}. \tag{B11}$$

The results are the same as that obtained by Ref. 20.

APPENDIX C: CORRELATION FUNCTIONS

The partial differential cross section in Eq. (32) involves summing α and β over x, y and z in the following expression:

$$\int_{-\infty}^{\infty} dt e^{-i\omega t}\left(\delta_{\alpha,\beta}-\hat{\boldsymbol{\kappa}}_{\alpha}\hat{\boldsymbol{\kappa}}_{\beta}\right)\sum_{\mathbf{mn}} e^{i\boldsymbol{\kappa}\cdot(\mathbf{m}-\mathbf{n})}\left\langle S^{\alpha}_{\mathbf{m}}\left(0\right)S^{\beta}_{\mathbf{n}}\left(t\right)\right\rangle.$$

We can now evaluate this expression for different values of α and β. Summing the expressions when $\alpha=\beta=x$ and $\alpha=\beta=y$ we get

$$\begin{aligned}
&\int_{-\infty}^{\infty} dt\, e^{-i\omega t}\sum_{\mathbf{mn}} e^{i\boldsymbol{\kappa}\cdot(\mathbf{m}-\mathbf{n})}\left[\left(1-\hat{\boldsymbol{\kappa}}_x^2\right)\left\langle S^x_{\mathbf{m}}\left(0\right)S^x_{\mathbf{n}}\left(t\right)\right\rangle+\left(1-\hat{\boldsymbol{\kappa}}_y^2\right)\left\langle S^y_{\mathbf{m}}\left(0\right)S^y_{\mathbf{n}}\left(t\right)\right\rangle\right]\\
&\quad=\frac{S}{2}\left(\hat{\boldsymbol{\kappa}}_y^2-\hat{\boldsymbol{\kappa}}_x^2\right)\int_{-\infty}^{\infty} dt e^{-i\omega t}{\sum_{\mathbf{mn}}}' e^{i\boldsymbol{\kappa}\cdot(\mathbf{m}-\mathbf{n})}\Big[\left\langle a^{\dagger}_{\mathbf{m}}(0)a^{\dagger}_{\mathbf{n}}(t)\right\rangle+\left\langle a_{\mathbf{m}}(0)a_{\mathbf{n}}(t)\right\rangle+\left\langle b^{\dagger}_{\mathbf{m}}(0)b^{\dagger}_{\mathbf{n}}(t)\right\rangle+\left\langle b_{\mathbf{m}}(0)b_{\mathbf{n}}(t)\right\rangle\\
&\qquad+\left\langle a^{\dagger}_{\mathbf{m}}(0)b_{\mathbf{n}}(t)\right\rangle+\left\langle a_{\mathbf{m}}(0)b^{\dagger}_{\mathbf{n}}(t)\right\rangle+\left\langle b^{\dagger}_{\mathbf{m}}(0)a_{\mathbf{n}}(t)\right\rangle+\left\langle b_{\mathbf{m}}(0)a^{\dagger}_{\mathbf{n}}(t)\right\rangle\Big]\\
&\quad+\frac{S}{2}\left(1+\hat{\boldsymbol{\kappa}}_z^2\right)\int_{-\infty}^{\infty} dt e^{-i\omega t}{\sum_{\mathbf{mn}}}' e^{i\boldsymbol{\kappa}\cdot(\mathbf{m}-\mathbf{n})}\Big[\left\langle a^{\dagger}_{\mathbf{m}}(0)a_{\mathbf{n}}(t)\right\rangle+\left\langle a_{\mathbf{m}}(0)a^{\dagger}_{\mathbf{n}}(t)\right\rangle+\left\langle b^{\dagger}_{\mathbf{m}}(0)b_{\mathbf{n}}(t)\right\rangle+\left\langle b_{\mathbf{m}}(0)b^{\dagger}_{\mathbf{n}}(t)\right\rangle\\
&\qquad+\left\langle a^{\dagger}_{\mathbf{m}}(0)b^{\dagger}_{\mathbf{n}}(t)\right\rangle+\left\langle a_{\mathbf{m}}(0)b_{\mathbf{n}}(t)\right\rangle+\left\langle b^{\dagger}_{\mathbf{m}}(0)a^{\dagger}_{\mathbf{n}}(t)\right\rangle+\left\langle b_{\mathbf{m}}(0)a_{\mathbf{n}}(t)\right\rangle\Big].
\end{aligned}\tag{C1}$$

where the primed sum indicates that $\mathbf{m}$ and $\mathbf{n}$ are on the A sublattice when the bosonic operator is a or $a^{\dagger}$ and on the B sublattice for the b and $b^{\dagger}$ operators. The Heisenberg representations of $a_{\mathbf{r}}$ and $b_{\mathbf{r}}$ are given by

$$a_{\mathbf{r}} = \sum_{\mathbf{q}}\frac{e^{i\mathbf{q}\cdot\mathbf{r}}}{\sqrt{N}}\Big[u_1\left(\mathbf{q}\right)e^{-i\omega_1(\mathbf{q})t}\alpha_{\mathbf{q}}+v_1\left(\mathbf{q}\right)e^{-i\omega_2(\mathbf{q})t}\beta_{\mathbf{q}}+u_2\left(\mathbf{q}\right)e^{i\omega_1(\mathbf{q})t}\alpha^{\dagger}_{-\mathbf{q}}+v_2\left(\mathbf{q}\right)e^{i\omega_2(\mathbf{q})t}\beta^{\dagger}_{-\mathbf{q}}\Big],\tag{C2}$$

$$b_{\mathbf{r}} = \sum_{\mathbf{q}}\frac{e^{-i\mathbf{q}\cdot\mathbf{r}}}{\sqrt{N}}\Big[-u_2\left(\mathbf{q}\right)e^{i\omega_1(\mathbf{q})t}\alpha^{\dagger}_{\mathbf{q}}+v_2\left(\mathbf{q}\right)e^{i\omega_2(\mathbf{q})t}\beta^{\dagger}_{\mathbf{q}}-u_1\left(\mathbf{q}\right)e^{-i\omega_1(\mathbf{q})t}\alpha_{-\mathbf{q}}+v_1\left(\mathbf{q}\right)e^{-i\omega_2(\mathbf{q})t}\beta_{-\mathbf{q}}\Big].\tag{C3}$$

The correlation function $\left\langle a_{\mathbf{m}}\left(0\right)a^{\dagger}_{\mathbf{n}}\left(t\right)\right\rangle$ occurring in Eq. (C1) is given by

$$\begin{aligned}
\left\langle a_{\mathbf{m}}\left(0\right)a^{\dagger}_{\mathbf{n}}\left(t\right)\right\rangle &= \frac{1}{N}\sum_{\mathbf{q}}e^{i\mathbf{q}\cdot(\mathbf{m}-\mathbf{n})}\Big[u_1^2\left(\mathbf{q}\right)e^{i\omega_1(\mathbf{q})t}\left(\eta\left(\omega_1\right)+1\right)+u_2^2\left(\mathbf{q}\right)e^{-i\omega_1(\mathbf{q})t}\eta\left(\omega_1\right)\\
&\qquad+v_1^2\left(\mathbf{q}\right)e^{i\omega_2(\mathbf{q})t}\left(\eta\left(\omega_2\right)+1\right)+v_2^2\left(\mathbf{q}\right)e^{-i\omega_2(\mathbf{q})t}\eta\left(\omega_2\right)\Big],
\end{aligned}\tag{C4}$$

where $\eta\left(\omega\right)$ is the Bose distribution function. Hence,

$$\begin{aligned}
&\int_{-\infty}^{\infty} dt e^{-i\omega t}\sum_{\substack{\mathbf{m}\in A\\ \mathbf{n}\in A}} e^{-i\boldsymbol{\kappa}\cdot(\mathbf{m}-\mathbf{n})}\left\langle a_{\mathbf{m}}\left(0\right)a^{\dagger}_{\mathbf{n}}\left(t\right)\right\rangle=\\
&\quad\frac{\left(2\pi\right)^3}{v_0}\int\frac{d^3q}{\left(2\pi\right)^3}\sum_{\boldsymbol{\tau}}\Big(\delta\left(\boldsymbol{\kappa}-\mathbf{q}-\boldsymbol{\tau}\right)\left[u_1^2\left(\mathbf{q}\right)\delta\left(\omega-\omega_1\right)\left(\eta\left(\omega_1\right)+1\right)+v_1^2\left(\mathbf{q}\right)\delta\left(\omega-\omega_2\right)\left(\eta\left(\omega_2\right)+1\right)\right]\\
&\qquad+\delta\left(\boldsymbol{\kappa}+\mathbf{q}-\boldsymbol{\tau}\right)\left[u_2^2\left(\mathbf{q}\right)\delta\left(\omega+\omega_1\right)\eta\left(\omega_1\right)+v_2^2\left(\mathbf{q}\right)\delta\left(\omega+\omega_2\right)\eta\left(\omega_2\right)\right]\Big),
\end{aligned}\tag{C5}$$

where $\boldsymbol{\tau}$ is a reciprocal lattice vector. The remaining correlation functions in Eq. (C1) are evaluated in the same manner. Similarly, one can calculate the terms corresponding to the position and time Fourier transforms for the other spin-spin correlation functions, however, the remaining correlation functions do not contribute to the

partial differential cross section.

[1] R. Moessner and S. L. Sondhi, Phys. Rev. Lett. **86**, 1881 (2001).
[2] P. W. Anderson, Mater. Res. Bull. **8**, 153 (1973).
[3] P. Fazekas and P. W. Anderson, Philos. Mag. **30**, 423 (1974).
[4] X. Wen, Adv. Phys. **44**, 405 (1995).
[5] R. Coldea, D. A. Tennant, and Z. Tylczynski, Phys. Rev. B **68**, 134424 (2003).
[6] R. Coldea, D. A. Tennant, A. M. Tsvelik, and Z. Tylczynski, Phys. Rev. Lett. **86**, 1335 (2001).
[7] Y. Shimizu *et al.*, Phys. Rev. Lett. **91**, 107001 (2003).
[8] K. Shimizu *et al.*, cond-mat/0604650 (2006).
[9] F. Vernay, K. Penc, P. Fazekas, and F. Mila, Phys. Rev. B **70**, 014428 (2004).
[10] Y. Kitaoka *et al.*, J. Phys. Soc. Jap. **67**, 3703 (1998).
[11] K. Hirakawa, H. Kadowaki, and K. Ubukoshi, J. Phys. Soc. Jap. **54**, 3526 (1985).
[12] E. Chappel *et al.*, Eur. Phys. J. B **17**, 609 (2000).
[13] E. Chappel *et al.*, Phys. Rev. B **66**, 132412 (2002).
[14] A. Rougier, C. Delmas, and A. Chadwick, Solid State Commun. **94**, 123 (1995).
[15] J.-H. Chung *et al.*, Phys. Rev. B **71**, 064410 (2005).
[16] J. N. Reimers *et al.*, J. Solid State Chem. France **102**, 542 (1993).
[17] J. Goodenough, *Magnetism and the Chemical Bond* (Interscience Publishers, New York-London, 1963).
[18] M. Holzapfel *et al.*, Phys. Rev. B **70**, 132410 (2004).
[19] M. J. Lewis *et al.*, Phys. Rev. B **72**, 014408 (2005).
[20] R. Schmitz *et al.*, Phys. Rev. B **71**, 214438 (2005).
[21] R. Schmitz, O. Entin-Wohlman, A. Aharony, and E. Müller-Hartmann, cond-mat/0506328 (2005).
[22] T. Yildirim, A. B. Harris, A. Aharony, and O. Entin-Wohlman, Phys. Rev. B **52**, 10239 (1995).
[23] T. Yildirim, A. B. Harris, O. Entin-Wohlman, and A. Aharony, Phys. Rev. Lett. **73**, 2919 (1994).
[24] I. Dzyaloshinskii, J. Phys. Chem. Solids **4**, 241 (1958).
[25] H. Eskes and J. H. Jefferson, Phys. Rev. B **48**, 9788 (1993).
[26] J. Griffith, *The Theory of Transition Metal Ions* (Cambridge University Press, London, 1961).
[27] J. van Elp, H. Eskes, P. Kuiper, and G. A. Sawatzky, Phys. Rev. B **45**, 1612 (1992).
[28] E. Clementi and C. Roetti, At. Data Nucl. Data Tables **14**, 177 (1974).
[29] J. C. Slater and G. F. Koster, Phys. Rev. **94**, 1498 (1954).
[30] M. Takahashi, J. Phys. C **10**, 1289 (1977).
[31] R. White, M. Sparks, and I. Ortenburger, Phys. Rev. **139**, A450 (1965).
[32] M. Enjalran and M. J. Gingras, Phys. Rev. B **70**, 174426 (2004).